# Ti17 合金惯性摩擦焊接头力学性能与组织分析

许鸿吉[1]， 尹丽香[2]， 魏志宇[3]， 谢 明[1]， 张田仓[4]

（1. 大连交通大学 材料科学与工程学院，辽宁 大连 116028；
2. 林德工程(大连)有限公司，辽宁 大连 116113；
3. 大连中集集装箱有限公司，辽宁 大连 116600；4. 北京航空制造工程研究所，北京 100024）

许鸿吉

摘 要：通过室温拉伸、高温拉伸试验以及金相分析对 Ti17 合金惯性摩擦焊接接头的显微组织和力学性能进行了研究. 结果表明，采用惯性摩擦焊焊接 Ti17 合金可获得室温及高温性能良好的焊接接头，其焊接接头的室温及高温抗拉强度都不低于母材；Ti17 合金母材组织为 α+β 相，并且 β 相呈针状均匀分布在 α 相的基体上；不同焊接工艺参数对 Ti17 合金惯性摩擦焊接头热影响区和焊缝的组织没有影响，其热影响区组织为 α+β 相，并且 β 相呈针状均匀分布在 α 相的基体上，与母材组织相同，焊缝组织为细小的等轴晶.

关键词：Ti17 合金；惯性摩擦焊；室温拉伸；高温拉伸
中图分类号：TG457.19 文献标识码：A 文章编号：0253－360X(2009)12－0089－04

## 0 序 言

Ti17(Ti-5Al-2Sn-2Zr-4Mo-4Cr)合金是一种富 β 稳定元素的 α-β 型两相钛合金，该合金具有强度高、断裂韧度好、淬透性高和锻造温度宽等一系列优点，能够满足损伤容限设计的需要和高结构效益、高可靠性及低制造成本的要求. 在航空工业中得到较为广泛的应用[1,2]. 20 世纪 90 年代，西方发达国家将研制出的高强度钛合金(Ti-5Al-2Sn-2Zr-4Mo-4Cr)，通过整体锻造＋数控加工应用于新型航空发动机叶轮部件，显著提高了发动机的效率[3].

摩擦焊具有广泛的工艺适应性、焊接过程可靠性高、焊件尺寸精度较高等技术优势，是一种优质、高效、低耗、清洁的先进焊接制造工艺，在高新技术产业和传统产业部门具有巨大的技术潜力和广阔的市场前景. 惯性摩擦焊作为摩擦焊的一种，除了具有摩擦焊的一般优势外，还具有控制参数少(只有压力和转速)，便于实现自动控制；焊接参数稳定性好，接头质量稳定；能在短时间内释放较大能量，适于焊接大截面结构；焊接周期短，热影响区窄；不需要制动装置，焊机结构简单等优点，是大截面旋转体构件实现对接的首选方法. 因此，研究 Ti17 合金大截面构件惯性摩擦焊接头性能是十分必要的，具有十分重要的现实意义.

收稿日期：2008－08－22

## 1 试验方法

试验材料为 Ti17 合金管材，规格为 φ80 mm× 25 mm，焊前 Ti17 合金母材热处理状态为锻态下时效处理. 采用 Model300 SN 30XHLF2807 型惯性摩擦焊机进行焊接，分别进行了不同转速和不同压力下的惯性摩擦焊工艺试验，焊接工艺参数如表 1 所示. 焊后接头热处理状态为加热 630 ℃，时效时间 8 h 后空冷. 然后按航空标准进行室温及高温拉伸试验，试样形状及尺寸见图 1，焊缝位于试样的中间. 高温拉伸试验温度为 400 ℃. 拉伸试验在 ZWICK100KN 电子万能材料试验机上进行.

表 1 Ti17 合金惯性摩擦焊焊接工艺参数

Table 1 Inertia friction welding (IFW) parameters of Ti17 alloy

| 试件编号 | 压力 $p$/MPa | 转速 $n$/(r·min$^{-1}$) | 惯量 $J$/(kg·m$^{-2}$) |
|---|---|---|---|
| 1 | 7.58 | 1 500 | 10.87 |
| 2 | 7.58 | 900 | 10.87 |
| 3 | 7.58 | 700 | 10.87 |
| 4 | 6.55 | 1 500 | 10.87 |
| 5 | 6.55 | 900 | 10.87 |
| 6 | 6.55 | 700 | 10.87 |
| 7 | 5.52 | 1 500 | 10.87 |
| 8 | 5.52 | 900 | 10.87 |
| 9 | 5.52 | 700 | 10.87 |

用 JSM －6360LV 型扫描电镜分别对 Ti17 合金

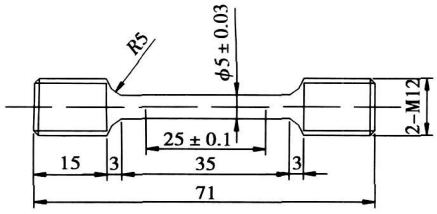


图 1 圆形带螺纹拉伸试样尺寸(mm)

Fig. 1 Dimension of tensile test specimen

惯性摩擦焊接头室温拉伸和高温拉伸试验断口进行了断口形貌观察. 对 Ti17 合金惯性摩擦焊接头在横截面方向截取金相试样,焊接接头位于试样中心部位.

## 2 试验结果与分析

### 2.1 焊接接头宏观形貌分析

图 2 为采用表 1 焊接工艺参数得到的 Ti17 合金惯性摩擦焊接头宏观形貌. 其中横向为压力和惯量一定,转速不同;纵向为转速和惯性一定,压力不同. 从图 2 中可以看出压力和惯量一定,随着转速降低,其接头处飞边和挤出量明显减少. 而转速和惯量一定时,压力对 Ti17 合金惯性摩擦焊接头宏观形貌影响不大. 不同压力下,各接头处的挤出量相差无几,其接头的飞边也大致相同.

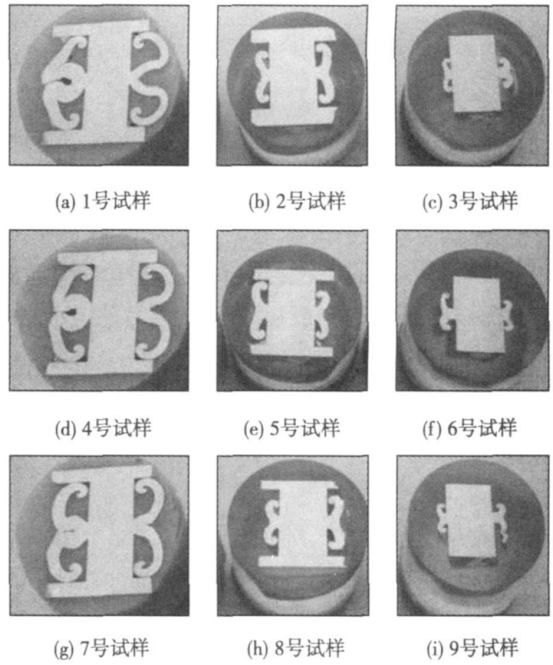


图 2 焊接接头宏观形貌

Fig. 2 Macro-appearance of welded joints

### 2.2 拉伸试验结果及分析

表2为Ti17合金母材及惯性摩擦焊接头拉伸试验结果. 从表 2 中可以看出 Ti17 合金不同焊接工艺参数下的焊接接头室温拉伸试验和高温拉伸试验结果都很集中,各焊接工艺下焊接接头的室温及高温抗拉强度均与母材抗拉强度相当. 通过对拉伸试样断裂部位的观察,可以看出,Ti17 合金惯性摩擦焊接头室温及高温拉伸时,其断裂部位均在距焊缝中心较远的母材上. 因此,说明采用惯性摩擦焊方法焊接 Ti17 合金可以获得优质的焊接接头,且焊接工艺参数可在较大的范围内变化.

表 2 Ti17 合金母材及惯性摩擦焊接头拉伸试验结果

Table 2 Results of tensile test of Ti17 alloy and IFW welded joints

| 材料 | 试样编号 | 室温拉伸试验(23 ℃) 抗拉强度 $R_m$/MPa | 规定非比例延伸强度 $R_{p0.2}$/MPa | 断后伸长率 $A$(%) | 断面收缩率 $Z$(%) | 拉断位置 | 高温拉伸试验(400 ℃) 抗拉强度 $R_m$/MPa | 规定非比例延伸强度 $R_{p0.2}$/MPa | 断后伸长率 $A$(%) | 断面收缩率 $Z$(%) | 拉断位置 |
|---|---|---|---|---|---|---|---|---|---|---|---|
| 母材 | M | 1 115 | 1 075 | 14.53 | 31.56 | — | 908 | 807 | 17.39 | 56.56 | — |
| 焊接接头 | 1 | 1 121 | 1 076 | 11.97 | 24.40 | 母材 | 912 | 824 | 16.19 | 45.11 | 母材 |
| | 2 | 1 125 | 1 072 | 12.70 | 28.94 | 母材 | 913 | 828 | 15.93 | 48.63 | 母材 |
| | 3 | 1 125 | 1 082 | 12.27 | 29.27 | 母材 | 910 | 823 | 15.49 | 45.54 | 母材 |
| | 4 | 1 119 | 1 057 | 15.20 | 33.45 | 母材 | 913 | 816 | 16.11 | 51.15 | 母材 |
| | 5 | 1 127 | 1 075 | 14.25 | 31.61 | 母材 | 914 | 815 | 16.03 | 51.58 | 母材 |
| | 6 | 1 128 | 1 063 | 15.34 | 26.29 | 母材 | 910 | 842 | 15.37 | 50.25 | 母材 |
| | 7 | 1 128 | 1 075 | 14.32 | 34.46 | 母材 | 917 | 852 | 15.36 | 50.53 | 母材 |
| | 8 | 1 140 | 1 096 | 12.86 | 29.69 | 母材 | 931 | 852 | 15.37 | 52.00 | 母材 |
| | 9 | 1 140 | 1 104 | 12.63 | 29.79 | 母材 | 916 | 849 | 15.00 | 52.86 | 母材 |

通过观察 Ti17 合金母材及惯性摩擦焊接头室温拉伸断口边缘及中心部位的断口形貌发现,Ti17 合金母材及惯性摩擦焊接头室温及高温拉伸断口边缘部位和中心部位的断口形貌均为浅韧窝,且边缘部位的浅韧窝比中心部位要浅一些,如图 3 和图 4 所示.

从断口形貌可以看出,Ti17合金惯性摩擦焊接

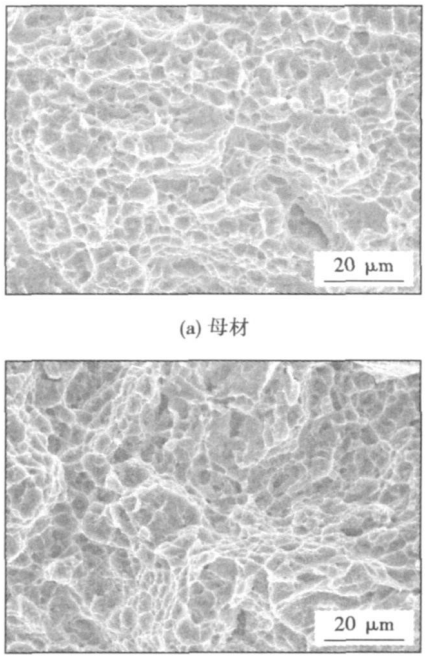


(a) 母材

(b) 焊接接头

图 3　Ti17 合金室温拉伸断口形貌

Fig. 3　Fracture appearances of Ti17 alloy room-temperature tensile specimens

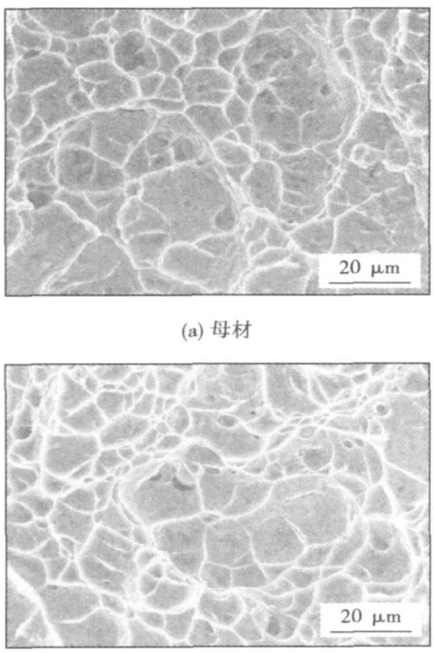


(a) 母材

(b) 焊接接头

图 4　Ti17 合金高温拉伸断口形貌

Fig. 4　Fracture appearances of Ti17 alloy high-temperature tensile specimens

头拉伸断口形貌受焊接工艺参数的影响不大，这主要是因为各焊接工艺参数下的 Ti17 合金惯性摩擦焊接头的抗拉强度均不低于母材，使得拉伸时断裂发生在距焊缝中心较远的母材上，其焊接接头的拉伸断口实际上就是母材拉伸的断口．因此，Ti17 合金母材与惯性摩擦焊接头拉伸断口形貌基本相同．

### 2.3　显微组织分析

通过金相显微镜和扫描电镜对 Ti17 合金惯性摩擦焊接头的显微组织进行观察发现，不同焊接工艺参数对 Ti17 合金惯性摩擦焊接头的显微组织影响不大．图 5 为 Ti17 合金惯性摩擦焊接头 1 号试样的显微组织形貌．

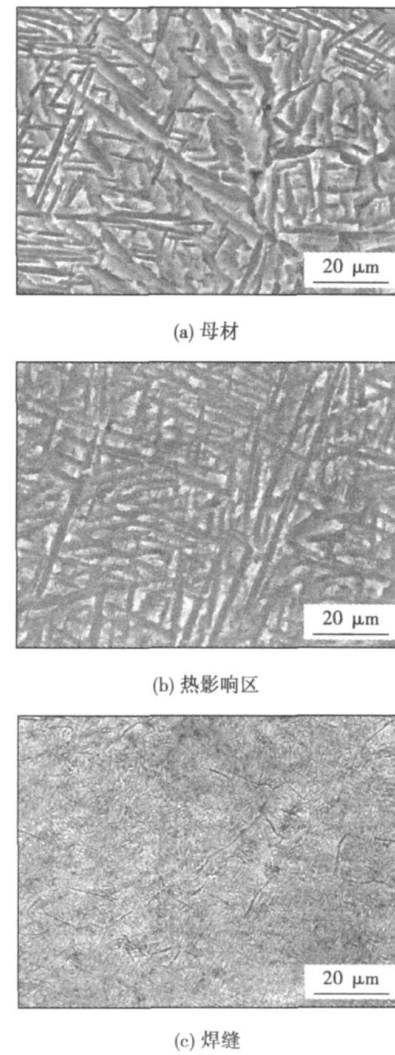


(a) 母材

(b) 热影响区

(c) 焊缝

图 5　Ti17 合金惯性摩擦焊接头 1 号试样显微组织形貌

Fig. 5　Microstructure for Specimen 1 of Ti17 alloy IFW joints

图 6 是 Ti17 合金惯性摩擦焊接头 9 号试样的显微组织形貌．从图 6 中可以看出，不同焊接工艺下焊接接头的热影响区组织与 Ti17 合金母材组织相差不大，均为 α＋β 相，并且 β 相呈针状均匀分布在

α 相的基体上, 没有晶粒长大现象. 焊缝区组织为细小的等轴晶, 其晶粒度远比母材小.

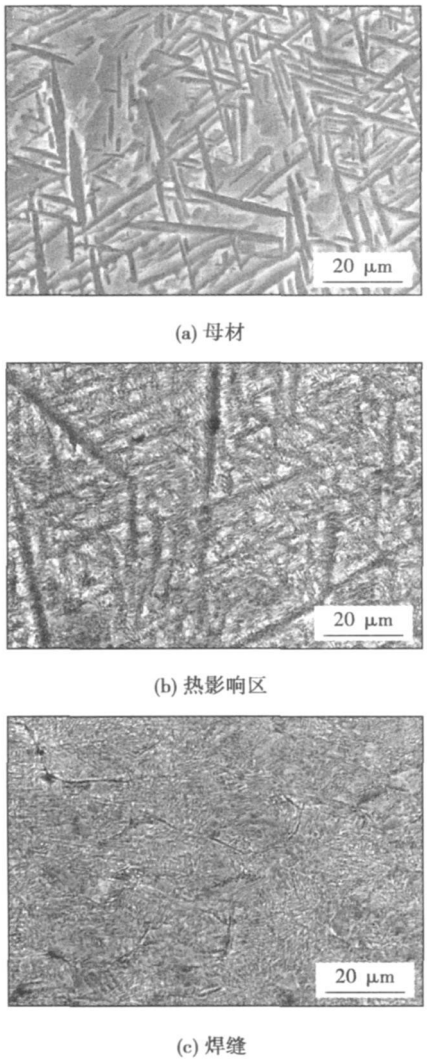


图 6 Ti17 合金惯性摩擦焊接头 9 号试样显微组织形貌

Fig. 6 Microstructure for Specimen 9 of Ti17 alloy IFW joints

## 3 结 论

(1) Ti17 合金惯性摩擦焊接头宏观形貌与焊接旋转速度有很大关系, 压力和惯量一定时, 转速越大, 接头的飞边和挤出量则越多. 而转速和惯量一定时, 压力对 Ti17 合金惯性摩擦焊接头飞边和挤出量的影响不大.

(2) Ti17 合金惯性摩擦焊接头室温及高温拉伸抗拉性能均与母材相当. 焊接接头拉伸试样断裂部位均在距焊缝中心较远的母材上.

(3) Ti17 合金母材组织为 α+β 相, 并且 β 相呈针状均匀分布在 α 相的基体上. 不同焊接工艺参数对 Ti17 合金惯性摩擦焊接头热影响区和焊缝的组织没有影响, 其热影响区组织为 α+β 相, 并且 β 相呈针状均匀分布在 α 相的基体上, 与母材组织相同, 焊缝组织为细小的等轴晶.

参考文献:

[1] Kurt H W. Titanium alloy are stronger and resist higher temperature [J]. Metal Engineering, 1973, 177(5): 52—55.

[2] 曾卫东, 胡鲜红, 于汉清, 等. Ti17 合金高温变形机理研究 [J]. 材料工程, 1996(9): 27—30.
Zeng Weidong, Hu Xianhong, Yu Hanqing, *et al*. An investigation on hot deformation mechanism of Ti17 alloy[J]. Material Engineering, 1996(9): 27—30.

[3] 周荣林, 郭德伦, 李从卿. 高强度钛合金 TIG 焊接[J]. 焊接, 2004(11): 29—31.
Zhou Ronglin, Guo Delun, Li Congqing. TIG welding of high strength titanium alloy[J]. Welding & Joining, 2004(11): 29—31.

作者简介: 许鸿吉, 男, 1959 年出生, 博士, 教授, 硕士研究生导师. 主要研究方向为先进连接技术. 发表论文 20 余篇.

Email: xuhongji@djtu.edu.cn

by using blowhole resistance as function and computer software, and then the trend diagrams of effects of every ingredient and the mathematical model between blowhole resistance of stainless steel electrode and 11 coating components were given. The effect of feldspar and muscovite on the mark of blowhole resistance is positive by trend diagrams. There are interactions between most coating components and blowhole resistance by mathematical model. The searching and forecasting can be done by using mathematical model and computer program.

**Key words**: stainless steel electrode; new slag system; blowhole; uniform design

**Numerical simulation on thermal fatigue behavior of CuCGA soldered joints** XIAO Zhengxiang[1], XUE Songbai[1], JIN Chunyu[2], ZHANG Liang[1], GAO Lili[1] (1. College of Materials Science and Technology, Nanjing University of Aeronautics and Astronautics, Nanjing 210016, China; 2. College of Mathematical Sciences, Heilongjiang University, Haerbin 150080, China). p 77—81

**Abstract**: The constitutive equation of Sn3.9Ag0.6Cu and 63Sn37Pb were established based on creep law, and the stress-strain distribution of soldered joints in copper column grid array (CuCGA) devices was analyzed under the loadings of different temperature cycles. Results indicate that no matter how the change of temperature cycle range, the maximum creep strain is located in the soldered joint where the location from the device center is foremost, in which the stress concentration is found and cracks appear; therefore, the corner soldered joint is the most fragile area in the whole device. Creep strain of Sn3.9Ag0.6Cu soldered joints is smaller than that of 63Sn37Pb soldered joints. Lower stress and creep strain are exhibited for both Sn3.9Ag0.6Cu and 63Sn37Pb when the temperature cycles range is shortened. Sn3.9Ag0.6Cu soldered joints show higher thermal fatigue life than 63Sn37Pb soldered joints under the same temperature cycle.

**Key words**: copper column grid array; reliability; creep law; fatigue life

**Formability and microstructure characteristics of galvanized plate by TIG welding** PENG Bendong[1], ZHANG Jian[1], LI Yuntao[1], YANG Lijun[2], LIU Guangda[1] (1. School of Materials Science and Engineering, Tianjin University of Technology, Tianjin 300191, China; 2. School of Materials Science and Engineering, Tianjin University, Tianjin 300191, China). p 82—84

**Abstract**: The microstructure and micro-hardness of welded joint of SGCC by tungsten inert-gas (TIG) welding are studied, and the cupping test of Tailor-welded blank and base metal are studied. The results show that in the welding process, the microstructure of weld will have great diversity at local region closing parent metal because of the different cooling condition of the parent metal. The microstructure of welding fusion zone is massive sheet proeutectoid ferrite distribution along the columnar grain boundaries, intragranular organizations are Widmanstatten and sheet pearlite structure, and the microstructure in HAZ is massive pearlite and ferrite, which make the micro-hardness value of welding seam and HAZ higher than that of base metal and lead negative influence to the formability of Tailor-welded blank. The cupping value of weld seam reduces to some extent compared with that of base metal, which indicates that the formability of weld seam is not good as that of base metal.

**Key words**: galvanized sheet; TIG welding; microstructures; cupping test

**Welding experiment on 1Cr18Ni9Ti and 1Cr13 stainless steels** ZHAO Yongtao[1], DONG Junhui[2], ZHAO Liping[1], MA Yonglin[1], PEI Xiaobing[1] (1. Material and Metallurgy Engineering School, UST Inner Mongolia, Baotou 014010, China; 2. Materials Science and Engineering, Inner Mongolia University of Technology, Huhhot 010051, China). p 85—88

**Abstract**: The stainless steels of 1Cr18Ni9Ti and 1Cr13 were welded through deterministic craft by tungsten inert-gas (TIG) welding. The microstructure and fracture pattern of weld joints of 1Cr13 martensite and 1Cr18Ni9Ti austenite stainless steels were observed and analyzed by means of LOM and SEM, the mechanical properties of the weld joints were measured with micro-hardness tester and electronic universal stretcher, and the polarization curves and AC impedance spectroscopy of weld joints were tested by seawater immersion test of simulation solution. The results show that adopting manual TIG welding through electrode negative to direct current soldering machine to weld 1Cr18Ni9Ti austenite stainless steel and 1Cr13 martensite stainless steel is feasible; under suitable process (welding current is 80 A, welding speed is 110 mm/min), weld joints can obtain good appearance and uniform structure; mechanical properties and galvano-chemistry properties can meet use requirements.

**Key words**: 1Cr13; 1Cr18Ni9Ti; welding joint; microstructure and properties

**Microstructures and properties of Ti17 alloy inertia friction welded joints** XU Hongji[1], YIN Lixiang[2], WEI Zhiyu[3], XIE Ming[1], ZHANG Tiancang[4] (1. School of Materials Science and Engineering, Dalian Jiaotong University, Dalian 116028, China; 2. Linde Engineering (Dalian) Co., Ltd, Dalian 116113, China; 3. Dalian CIMC Containers Co., Ltd, Dalian 116600 China; 4. Beijing Aeronautical Manufacturing Technology Research Institute, Beijing 100024, China). p 89—92

**Abstract**: The microstructures and properties of Ti17 alloy joints welded by inertia friction welding (IFW) were investigated by room-temperature tensile test, high-temperature tensile test and metallographic analyses. The results show that the joint with good performance at room and high temperature for Ti17 alloy can be obtained in IFW. Both the tensile strengths of welded joints at room temperature and at high temperature are not less than those of the base metal. The microstructure of Ti17 alloy is $\alpha+\beta$ phase, and the needle $\beta$ phase is distributing on the $\alpha$ phase. While welding, different welding parameters can not affect the microstructures of the HAZ and the weld seam. The microstructure of HAZ is the same as that of the base metal, and that of the welded seam is fine equiaxed crystal.

**Key words**: Ti17 alloy; inertia friction welding; room-temperature tensile test; high-temperature tensile test